



HAL
open science

Liquid B₂O₃ up to 1700 K: x-ray diffraction and boroxol ring dissolution

O. L. G. Alderman, G. Ferlat, A. Baroni, M. Salanne, M. Micoulaut, C. J. Benmore, A. Lin, A. Tamalonis, J. K. R. Weber

► To cite this version:

O. L. G. Alderman, G. Ferlat, A. Baroni, M. Salanne, M. Micoulaut, et al.. Liquid B₂O₃ up to 1700 K: x-ray diffraction and boroxol ring dissolution. *Journal of Physics: Condensed Matter*, 2015, 27 (45), pp.455104. 10.1088/0953-8984/27/45/455104 . hal-01502196

HAL Id: hal-01502196

<https://hal.science/hal-01502196v1>

Submitted on 19 Dec 2018

HAL is a multi-disciplinary open access archive for the deposit and dissemination of scientific research documents, whether they are published or not. The documents may come from teaching and research institutions in France or abroad, or from public or private research centers.

L'archive ouverte pluridisciplinaire **HAL**, est destinée au dépôt et à la diffusion de documents scientifiques de niveau recherche, publiés ou non, émanant des établissements d'enseignement et de recherche français ou étrangers, des laboratoires publics ou privés.

Liquid B₂O₃ up to 1700 K: x-ray diffraction and boroxol ring dissolution

O L G Alderman^{1,2}, G Ferlat³, A Baroni^{3,4,5}, M Salanne⁴, M Micoulaut⁵,
C J Benmore², A Lin^{1,6}, A Tamalonis¹ and J K R Weber^{1,2}

¹ Materials Development, Inc., Arlington Heights, IL 60004, USA

² X-Ray Science Division, Advanced Photon Source, Argonne National Laboratory, Argonne, IL 60439, USA

³ Sorbonne Universités, UPMC Université Paris 06, UMR 7590, IMPMC, F-75005 Paris, France

⁴ Sorbonne Universités, UPMC Université Paris 06, UMR 8234, PHENIX, F-75005 Paris, France

⁵ Sorbonne Universités, UPMC Université Paris 06, UMR 7600, LPTMC, F-75005 Paris, France


⁶ Department of Materials Science and Engineering, McCormick School of Engineering and Applied Science, 2220 Campus Drive, Northwestern University, Evanston, IL 60208, USA

E-mail: o.alderman@gmail.com

Abstract

Using high energy x-ray diffraction, the structure factors of glassy and molten B₂O₃ were measured with high signal-to-noise, up to a temperature of $T = 1710(20)$ K. The observed systematic changes with T are shown to be consistent with the dissolution of hexagonal [B₃O₆] boroxol rings, which are abundant in the glass, whilst the high- T ($\gtrsim 1500$ K) liquid can be more closely described as a random network structure based on [BO₃] triangular building blocks. We therefore argue that diffraction data *are* in fact qualitatively sensitive to the presence of small rings, and support the existence of a continuous structural transition in molten B₂O₃, for which the temperature evolution of the 808 cm⁻¹ Raman scattering band (boroxol breathing mode) has long stood as the most emphatic evidence. Our conclusions are supported by both first-principles and polarizable ion model molecular dynamics simulations which are capable of giving good account of the experimental data, so long as steps are taken to ensure a ring fraction similar to that expected from Raman spectroscopy. The mean thermal expansion of the B-O bond has been measured directly to be $\alpha_{\text{BO}} = 3.7(2) \times 10^{-6} \text{ K}^{-1}$, which accounts for a few percent of the bulk expansion just above the glass transition temperature, but accounts for greater than one third of the bulk expansion at temperatures in excess of 1673 K.

Keywords: liquid structure, boron oxide, borate, aerodynamic levitation, laser heating, glass structure, molecular dynamics

 Online supplementary data available from stacks.iop.org/JPhysCM/27/455104/mmedia

(Some figures may appear in colour only in the online journal)

1. Introduction

Boron trioxide is an exceptional glass forming liquid that is not known to crystallize from the ambient pressure melt under any conditions [1]. Such behavior is presumably related to the unique local structure and network topology of B₂O₃, which is based on triangular [BO₃] motifs that can link together to form 3-membered, planar units known as boroxol rings. The percentage of boron atoms, f , contained within boroxol rings has been contested in the past [2–6],

but the present consensus is that the ambient pressure glass contains between ~60% and ~80% of B atoms within such rings. Such a consensus is supported by evidence from Raman spectroscopy [7, 8], inelastic neutron scattering [9], ¹¹B nuclear magnetic resonance (NMR) spectroscopy [10–14], ¹⁷O NMR [14, 15], first principles calculations [4, 16], statistical arguments [17–19] and, arguably, x-ray and neutron diffraction [20–28]. Controversy arose initially due to low fractions, $f < 37\%$, being derived from molecular dynamics (MD) modelling [29–40] (see [41] for a review)

and later reverse Monte Carlo (RMC) fits of 3D atomistic models to diffraction data [2, 3]. The former has been attributed primarily to the unrealistically large quench rates (short timescales) necessary in MD simulations [4, 41]. The RMC studies [2, 3] prompted Soper [42] to derive glass models with high and low f , fitted to x-ray and neutron diffraction data using empirical potential structure refinement (EPSR). His conclusion was that the diffraction data are insensitive to f , given that equally good fits could be obtained for both high and low boroxol ring fractions.

In this paper we address the sensitivity of diffraction data to boroxol rings by studying the x-ray structure factor, measured to high statistical accuracy, and with high real-space resolution, over a wide range of temperatures in the liquid and glassy state of B_2O_3 . Since Raman spectroscopic studies [7, 8] support a gradual dissolution of boroxol rings above the glass transition temperature, diffraction measurements of the liquid at different T should show systematic changes consistent with this, if they are at all sensitive to f . In a similar vein to recent neutron diffraction studies of B_2O_3 glass under high pressure [43], where boroxol ring dissolution also occurs, we support our measurements with the latest first-principles and polarizable ion model (PIM) MD simulations.

2. Background theory

In a scattering experiment, the x-ray structure factor, $S(Q) - 1$, is related to the measured differential x-ray scattering cross-section, $d\sigma(Q)/d\Omega$, by [44]

$$S(Q) - 1 = \left(\frac{d\sigma}{d\Omega}(Q) - \sum_i c_i f_i^2(Q) - \sum_i c_i C_i(Q) \right) \left(\sum_i c_i f_i(Q) \right)^{-2} \quad (1)$$

where c_i is the atomic fraction of element i , $f_i(Q)$ the x-ray atomic form factor and $C_i(Q)$ the Compton scattering contribution. Since the present high energy x-ray measurements are far from B and O absorption edges, dispersion terms in $f_i(Q)$ are neglected. $Q = (4\pi \sin\theta)/\lambda$ is related to the scattering angle, 2θ , and the x-ray wavelength, λ . Written in terms of the partial structure factors, $S_{ij}(Q) - 1$, between pairs of atoms $i-j$,

$$S(Q) - 1 = \sum_{i,j} W_{ij}(Q) (S_{ij}(Q) - 1) \quad (2)$$

where we define the pair weighting factors

$$W_{ij}(Q) = c_i c_j f_i(Q) f_j(Q) \left(\sum_i c_i f_i(Q) \right)^{-2} \quad (3)$$

Relative average values of the $W_{ij}(Q)$, and $W_{ij}(Q=0)$, are listed in table 1 and compared to the equivalent quantities for neutron diffraction. $S(Q) - 1$ is related by sine Fourier transform to the total correlation function,

$$T(r) = 4\pi\rho r \sum_{i,j} W_{ij}(Q=0) + \frac{2}{\pi} \int_0^{Q_{\max}} Q(S(Q) - 1) M(Q) \sin(rQ) dQ = T^0(r) + D(r), \quad (4)$$

Table 1. Relative weighting factors for pair terms in neutron and x-ray diffraction from B_2O_3 . The values for neutron diffraction assume a typical isotopic enrichment to 99.57 at.% ^{11}B . The values for x-ray diffraction are based on free atom form factors [85]. Angular braces denote an average over the Q range used in the present study, $0.41 \leq Q \leq 24.47 \text{ \AA}^{-1}$.

Pair $i-j$	Relative weighting (%)		
	ND (^{11}B)	XRD ($Q=0$)	$\langle XRD \rangle$
B-O + O-B	49.1	41.5	38.8
O-O	32.3	49.8	53.8
B-B	18.7	8.7	7.3

where $T^0(r) = 4\pi\rho r \sum_{i,j} W_{ij}(Q=0)$, r is the scalar interatomic distance, ρ is the atomic number density and $M(Q)$ is a modification function which can be chosen to reduce the effects of the finite limits ($0 < Q \leq Q_{\max}$) of the integral. Here we have made use of the Lorch function [45], $M(Q) = (Q_{\max}/\pi Q) \sin(\pi Q/Q_{\max})$ for $Q \leq Q_{\max}$ and $M(Q) = 0$ otherwise. The partial pair correlation functions, $t_{ij}(r) = 4\pi\rho c_j r g_{ij}(r)$, can be obtained using equation (4) and making the substitutions $T(r) \rightarrow t_{ij}(r)$, $\rho \rightarrow \rho c_j$ and $S(Q) \rightarrow S_{ij}(Q)$.

In the harmonic approximation, a single interatomic distance, r_{ij} , with a root-mean-square variation $\langle u_{ij}^2 \rangle^{1/2}$ contributes to $S(Q) - 1$ according to [46]

$$s_{ij}(Q) = n_{ij} c_i f_i(Q) f_j(Q) \frac{\sin(Qr_{ij})}{Qr_{ij}} \exp\left(-\frac{1}{2} \langle u_{ij}^2 \rangle Q^2\right) \left(\sum_i c_i f_i(Q) \right)^{-2}, \quad (5)$$

where n_{ij} is the coordination number—the number of atoms of type j about an atom of type i . Equation (5) has a real-space manifestation given by [47]

$$t_{ij}(r) = \frac{n_{ij}}{r_{ij} \sqrt{2\pi \langle u_{ij}^2 \rangle}} \exp\left(-\frac{(r-r_{ij})^2}{2 \langle u_{ij}^2 \rangle}\right) \otimes P_{ij}(r), \quad (6)$$

where convolution (denoted by \otimes) by the peak function

$$P_{ij}(r) = \frac{1}{\pi} \int_0^{Q_{\max}} W_{ij}(Q) M(Q) \cos(rQ) dQ \quad (7)$$

is necessary for direct comparison to experimental data.

3. Methods

3.1. X-ray diffraction

Diffraction measurements were performed at beamline 6-ID-D of the Advanced Photon Source (Argonne, IL, USA). A spheroidal glass sample approximately 3 mm in diameter was levitated in a stream of argon (99.999% pure) flowing through a converging-diverging aerodynamic nozzle. The sample was heated from above with a partially focused CO_2 laser beam. The incident heating power was adjusted to control the sample temperature, which was measured with a single colour pyrometer (Chino model IRCS) sighted onto the top of the sample where it was also being heated.

The apparent temperature was corrected using a Wien's displacement law approximation [48] with a spectral emissivity value of 0.969 for B_2O_3 at the pyrometer wavelength of $5.0 \mu\text{m}$. The emissivity value was calculated from the Fresnel losses for a material with a refractive index of 1.43, which is an estimated value based on the 589 nm refractive index of about 1.46 [49]. The pyrometer temperature was also corrected for reflection losses from a CaF_2 window and CaF_2 lens that were in the optical path. The temperature correction is relatively large due to the long wavelength of $5.0 \mu\text{m}$, but this was found necessary due to transparency of the sample at shorter infrared wavelengths. The (maximum) total correction amounts to 134 K at the maximum apparent temperature of 1573 K, and we estimate a true maximum temperature of 1707(24) K, with the quoted uncertainty arising from temperature fluctuations, in addition to the emissivity correction. Although there are top-to-bottom temperature gradients on the order of 100 K through the sample, by making both temperature and x-ray measurements at the top where it is heated, the temperature of the liquid being probed is relatively uniform. Structure was measured using a high energy (100.24 keV) x-ray beam with cross-section $500 \mu\text{m} \times 500 \mu\text{m}$ horizontally incident upon the top of the sample in the region where it was heated.

An area x-ray detector (Perkin Elmer XRD1621, 2048×2048 pixels of $200 \mu\text{m} \times 200 \mu\text{m}$ Tl doped CsI) was used. Sample to detector distance (381 mm) was calibrated using a polystyrene bead coated in polycrystalline CeO_2 powder, which was placed in the nozzle.

To obtain samples suitable for levitation, anhydrous B_2O_3 (Aldrich, 99.999%) was pre-melted in a platinum crucible at 1273 K for 60 mins, before quenching the crucible base into water. For reference, the glass transition temperature $T_g \approx 540$ K and liquidus temperature $T_l \approx 720$ K. Fragments of the obtained glass were then melted in a water-cooled copper hearth, using a 100 W CO_2 laser, and the surface tension of the melt relied upon to form roughly spherical beads. Sample contamination has been shown to be negligible by this method [50]. Samples were held in bottles purged with dry N_2 , inside a desiccator until required. The x-ray diffraction results shown are taken from two separate high temperature runs. After measuring the room temperature glass for two minutes, the first run involved heating to about 710 K, measuring the liquid diffraction pattern for two minutes, followed by stepwise increments of about 50 K of the sample temperature, up to a maximum of 1490 K, a total of 18 two-minute measurements on the liquid. The melt was then cooled in the same stepwise manner, again collecting diffraction patterns at each step and at room temperature. The average heating/cooling rate was $\sim 0.31 \text{ K s}^{-1}$. The reason for collecting data on both heating and cooling was to check for any structural changes due to evolution of absorbed water, as well as any other possible hysteretic behavior. The second run was similar, except the sample temperature was rapidly increased to 1530 K and five stepwise measurements made up to a maximum of 1710 K. At such high T , volatilization losses of the sample were large, and so no data were collected on cooling.

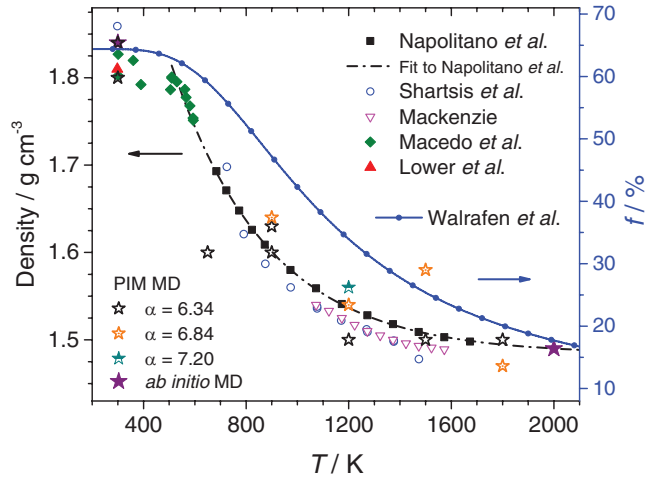


Figure 1. Measured densities of molten B_2O_3 [54, 55, 57, 80, 86] compared to MD model densities, and boroxol ring fraction, f , from Raman scattering (Walrafen *et al* [7]). The glass transition temperature is ≈ 540 K and the melting temperature ≈ 720 K.

The raw data were reduced from 2D images and corrected [51] for the effects of polarization, absorption, geometry and normalized using the programs Fit2d [52] and GudrunX [53]. In addition to these standard corrections, it was found that an additional additive background had to be subtracted from the data. We attribute this to a sample-dependent background arising from single scattering in the sample followed by 2nd scattering (mostly Compton) in the air and other absorber layers between sample and detector. This contribution was approximated as a constant level and does lead to some systematic error in the $S(Q)$ at values $Q < 1 \text{ \AA}^{-1}$. However, this uncertainty does not directly affect any of our analyses.

Density of the B_2O_3 melt was estimated by interpolation of the measurements made by Napolitano *et al* [54], using a fitted equation $\rho_m = 1.28 \exp(-T/377) + 1.484$ in K and g cm^{-3} , figure 1. The density of the glass was taken to be 1.81 g cm^{-3} [55].

3.2. Molecular dynamics

The aim of molecular dynamics is to provide realistic models obtained from atomistic simulations. From these, structural data (both in real and reciprocal space) can be computed and directly compared to experimental data. In the case of B_2O_3 , large structural changes (figure 1) occur in a temperature range (500–1300 K) where the viscosity increases by 12 orders of magnitude [54, 56–58]. From the MD point of view, this drastic increase impedes equilibration at low temperatures (typically below 1500 K) given the limited simulation times affordable [41]. Thus the strategy followed here, as in previous works [16, 43, 59], is to use different initial configurations and thermal histories to produce models containing various amounts of boroxol rings. These models, listed in table 2, can then be used to test the sensitivity of the x-ray data to the content of boroxol rings.

A series of samples were obtained from first-principles (based on density functional theory) MD simulations: these include the *boroxol-poor* ($f=22\%$) and *boroxol-rich* ($f=75\%$)

Table 2. Temperatures, densities and boroxol ring fractions of MD models, as compared to experimental values, along with $R\chi$ (equation (9)) and average B-O-B angles from MD (standard deviations in parentheses). Copyright 2000 Society of Glass Technology. Original data available as supplementary data (stacks.iop.org/JPhysCM/27/455104/mmedia).

T_{XRD} (K)	ρ^a (gcm ⁻³)	f^b (%)	T_{MD} (K)	ρ_{MD} (gcm ⁻³)	f_{MD} (%)	ΔT (K)	$\Delta\rho$ (gcm ⁻³)	Δf (%)	$R\chi^c$	$\langle\beta_{\text{R}}\rangle$ (°)	$\langle\beta_{\text{NR}}\rangle$ (°)
First-principles											
298	1.81	64	300	1.84	75	-2	-0.03	-11	8.1	118.7(3.0)	132.2(10.5)
298	1.81	64	300	1.84	61	-2	-0.03	3	4.9	118.7(2.9)	132.4(10.3)
298	1.81	64	300	1.84	22	-2	-0.03	42	7.0	118.6(3.1)	131.7(10.1)
1707	1.50	21	2000	1.49	23	-293	0.01	-2	3.3	116.8(8.1)	135.1(16.3)
PIM $\alpha = 6.34$											
298	1.81	64	300	1.84	75	-2	-0.03	-11	7.6	118.6(2.9)	129.7(6.8)
298	1.81	64	300	1.84	22	-2	-0.03	42	9.0	118.4(3.1)	129.8(8.2)
707	1.68	57	650	1.60	11	57	0.08	46	9.1	118.5(4.2)	129.3(8.7)
900	1.60	37	900	1.63	17	0	-0.03	20	6.9	118.3(5.0)	130.1(10.3)
900	1.60	37	900	1.60	5	0	0.00	32	8.3	118.3(4.9)	130.2(10.2)
1221	1.53	33	1200	1.50	7	21	0.03	27	7.8	117.9(5.7)	130.6(11.6)
1488	1.51	26	1500	1.50	10	-12	0.01	15	6.8	117.8(6.5)	131.2(12.7)
1707	1.50	21	1800	1.50	8	-93	-0.00	13	6.5	117.4(7.1)	131.4(13.6)
PIM $\alpha = 6.84$											
900	1.60	37	900	1.64	35	0	-0.04	2	6.5	116.4(5.0)	125.4(9.2)
1221	1.53	33	1200	1.48	29	21	-0.05	4	6.3	116.1(5.8)	126.2(10.6)
1488	1.51	26	1500	1.58	22	-12	-0.07	4	5.8	115.8(6.5)	126.6(11.8)
1707	1.50	21	1800	1.51	25	-93	0.01	-4	5.5	115.7(7.1)	127.2(12.8)
PIM $\alpha = 7.20$											
1221	1.53	33	1200	1.56	47	21	-0.03	-14	5.2	115.0(5.6)	124.1(10.1)

^a Interpolated from [54] using fitted equation $\rho_m = 1.28 \exp(-T/377) + 1.484$ in K and g cm⁻³ (figure 1). The density of the glass was taken to be 1.81 g cm⁻³ [55].

^b Calculated from Walrafen *et al*'s equation (2) [7] (figure 1, equation (10)).

^c Calculated over the range $2.65 \leq r \leq 5.00$ Å, sensitive to boroxol rings.

glassy models described previously [16] as well as a new one ($f = 61\%$) obtained from a liquid inherent structure (taken from figure 1 of [16]). In the liquid state, a 500 ps simulation of 100 atoms has been carried out at 2000 K and 1.49 g cm⁻³ with a technical set-up identical to that of [16].

In order to extend the systems sizes and simulation times, polarizable force-fields were derived using the methodology described in [60]: parameters related to the oxygen polarizability are calibrated from first-principles calculations of atomic forces and dipoles obtained in benchmark configurations. The parameterization [61] of the polarizable ion model (PIM) used in this work is similar to that of the aspherical ion model (AIM) used recently to simulate B₂O₃ glass under high pressures [43]. The simpler potential used here allows improved statistics (up to 340 ns per sample) which is compulsory because of the long equilibration times observed in B₂O₃ (see below). In the obtained PIM, the oxygen ion polarizability is $\alpha = 6.34$ (in atomic units). Previous simulation works [31, 41] have shown that boroxol ring formation is strongly affected by polarization effects in classical MD. Thus, in order to explore the influence of this parameter, two additional force-fields were generated by increasing the oxide polarizability α from its original value (6.34) to 6.84 and 7.2 a.u. while keeping all other parameters fixed.

A first series of liquid samples were generated with PIM MD starting with an initial cubic box of 800 atoms ($f = 22\%$) at 1800 K and 1.50 g cm⁻³. Typically, at each temperature

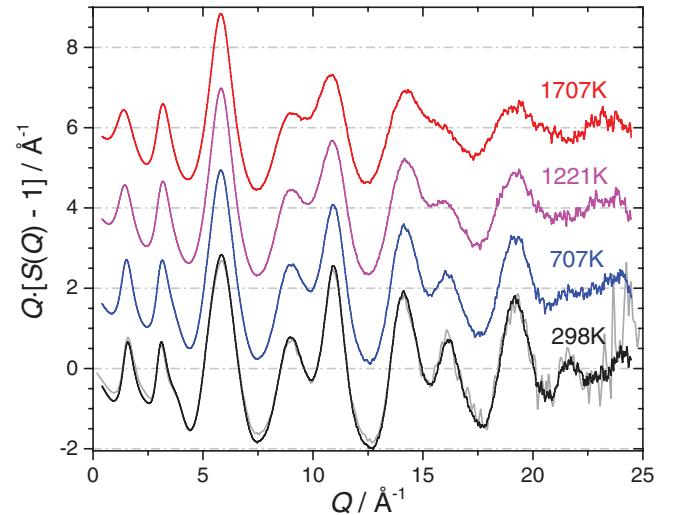


Figure 2. Representative interference functions for glassy B₂O₃ at 298 K and liquid B₂O₃ at various temperatures, as indicated. Vertical offsets have been applied for clarity. The light grey line superimposed on the 298 K data is from a previous synchrotron x-ray study of B₂O₃ glass [3]. Copyright 2000 Society of Glass Technology. Original data available as supplementary data (stacks.iop.org/JPhysCM/27/455104/mmedia).

considered (1800, 1500, 1200, 900, 650 K), the system is equilibrated for 10 ns after the density has been adapted to follow the experimental variation. The duration of a quench

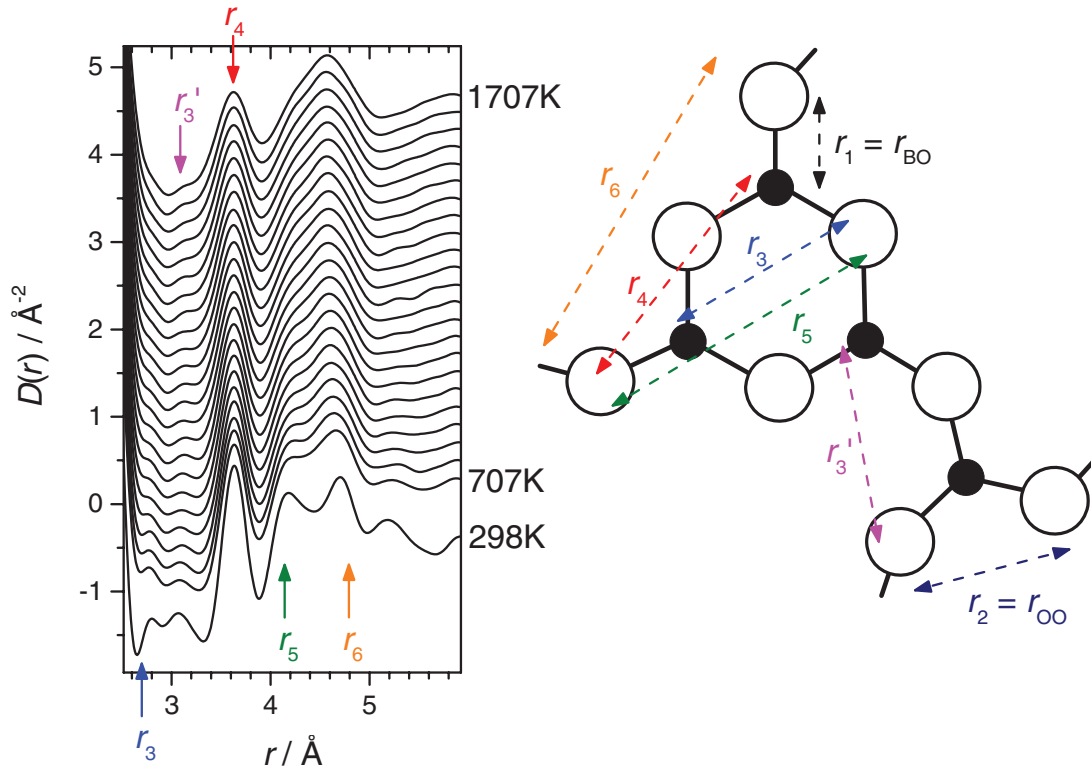


Figure 3. $D(r)$ ($Q_{\max} = 24.47 \text{ \AA}^{-1}$, with Lorch) for glassy B_2O_3 , and the liquid as a function of temperature, showing the intermediate range peaks. Vertical offsets have been applied for clarity. A schematic boroxol ring linked to a $[\text{BO}_3]$ triangle is shown to illustrate the various intraboroxol ring distances r_j , and a broken ring (intertriangle) distance r'_3 is also shown. Distances r_j refer to the special case where B-O-B bond angle $\beta = 120^\circ$, and the torsion angle $\phi = 0$ (see figure 4). Distances $r'_j(\beta, \phi)$ refer to the general case (see table 3, figure 4).

between the various temperatures is typically 10 to 30 ns, resulting in average quenching rates of $1.0\text{--}3.3 \times 10^{10} \text{ K s}^{-1}$. It should be stressed that these durations, although long enough at high temperatures ($\geq 1500 \text{ K}$) do not allow for a rigorous ergodic sampling at lower temperatures ($\leq 1200 \text{ K}$). Indeed, by monitoring the mean-squared displacement, it appeared that the diffusive regime could not be reached for $T \leq 1200 \text{ K}$ within our simulation times.

The f values (table 2) obtained from this series tend to underestimate the experimental ones from Raman scattering [7] (e.g. $f = 5\%$ instead of 37% [7] at 900 K), possibly reflecting an insufficient equilibration or a force-field deficiency. The *boroxol-rich* model (320 atoms, $f = 75\%$) has also been used as an initial configuration at 900 K : the resulting f value (17%) is however still too low.

Additional liquid samples were generated using the force-fields with increased polarizabilities. At each temperature, long *NPT* runs (typically 100–340 ns) were conducted starting from the *boroxol-rich* model. The obtained f values (table 2) are in very good agreement with the experimental ones.

4. Results

Representative interference functions, $Q \cdot (S(Q) - 1)$, covering the full temperature range explored are plotted in figure 2. Since no significant differences between data taken on heating and cooling were observed, the analyses presented herein are

based on data taken during heating only. As can be seen in figure 2, the room temperature data are in good agreement with a previous high-energy x-ray diffraction measurement of B_2O_3 glass [3]. Figure 3 shows the full set of $D(r)$ curves obtained upon heating, in the region beyond the 1st neighbor peaks. Some characteristic interatomic distances associated with boroxol rings are also indicated on the plot, and defined in the schematic (figure 3). Table 3 gives a description of these interatomic distances, which in general are denoted $r'_j(\beta, \phi)$ and are functions of the B-O-B angle β , and intertriangle dihedral angle ϕ (see figure 4). For the special case of boroxol rings, the distances are denoted simply by $r_j = r'_j(120^\circ, 0)$. We shall refer to the associated peak positions observed in the $D(r)$ by R_j . Note that the index j increases with interatomic distance, but that B-B distances have been ignored in the indexing owing to the small contribution of B-B pairs to the diffraction patterns.

The first two peaks in $T(r)$, at R_1 and R_2 , were fitted with profiles according to equations (6) and (7). The $T(r)$ for these purposes were obtained with a step modification function ($M(Q) = 1$ for $Q \leq Q_{\max}$ and 0 otherwise), and typically for $Q_{\max} = 24.47 \text{ \AA}^{-1}$. A model B-B peak with the following parameters was held fixed during the fitting procedure: $r_{\text{BB}} = 2.40 \text{ \AA}$, $\langle u_{\text{BB}}^2 \rangle^{1/2} = 0.070 \text{ \AA}$, $n_{\text{BB}} = 3$. Neglecting the temperature dependence of the B-B peak is an approximation that is somewhat justified by its small contribution to the total intensity, and allowed all parameters of the B-O and

Table 3. Interatomic distances within and between [BO₃] triangles and boroxol rings. See figures 3 and 4 for graphical depictions. Distances r_j refer to the special case where B-O-B bond angle $\beta = 120^\circ$, and the torsion angle $\phi = 0$ (see figure 4). Distances $r'_j(\beta, \phi)$ refer to the general case. Double angular parentheses denote a weighted average over β , using the reported non-ring B-O-B bond angle distribution for B₂O₃ glass [10], and an unweighted average over $\phi \in [0, \pi/2]$. Inequalities are based on $180^\circ > \beta > 120^\circ$.

Distance	Pair $i-j$	Type	n_{ij}	r_{ij}/r_1	r_{ij} (Å)	On ring breaking ($\beta > 120^\circ$)
r_1	B-O	Intratriangle	3	1	1.3765	-
r_2	O-O	Intratriangle	4	$\sqrt{3}$	2.384	$r_2 \rightarrow r_2$ & $r'_X \geq r_2$
r_{BB}	B-B	Intraring	$2f$	$\sqrt{3}$	2.384	$r_{BB} \rightarrow r'_{BB} \geq r_{BB}$
r_3	B-O	Intraring	f	2	2.753	$r_3 \rightarrow r'_3$ or $r''_3 \geq r_3$
r_4	B-O	Intraring	$2f$	$\sqrt{7}$	3.642	$r_4 \rightarrow r'_4$ or $r''_4 \approx r_4$
r_5	O-O	Intraring	$3f/2$	3	4.130	$r_5 \rightarrow r'_5$ or $r''_5 \geq r_5$
r_6	O-O	Intraring	$2f$	$2\sqrt{3}$	4.768	$r_6 \rightarrow r'_6 \leq r_6$
$\langle \langle r'_{ij} \rangle \rangle$ (Å) r'_{ij}/r_1						
r'_{BB}	B-B	Intertriangle	$3 - 2f$		2.540	$2\sin(\beta/2)$
r'_3	B-O	Intertriangle	$3/2 - f$		3.177	$(4 - 3\cos\beta - \sqrt{3}\sin\beta\cos\phi)^{1/2}$
r'_4	B-O	Intertriangle	$3/2 - f$		3.609	$(4 - 3\cos\beta + \sqrt{3}\sin\beta\cos\phi)^{1/2}$
r'_5	O-O	Intertriangle	$2 - 3f/2$		4.162	$(6 + (3/2)[\sqrt{3}\sin\beta(\cos\phi - 1) - \cos\beta(\cos\phi + 3)])^{1/2}$
r'_6	O-O	Intertriangle	$2 - 3f/2$		4.662	$(6 + (3/2)[\sqrt{3}\sin\beta(\cos\phi + 1) + \cos\beta(\cos\phi - 3)])^{1/2}$
r''_3	B-O	Intertriangle	$3/2 - f$		3.044	$(4 - \sqrt{3}[\sqrt{3}\cos\beta + \sin\beta])^{1/2}$
r''_4	B-O	Intertriangle	$3/2 - f$		3.725	$(4 - \sqrt{3}[\sqrt{3}\cos\beta - \sin\beta])^{1/2}$
r''_5	O-O	Intertriangle	$2 - 3f/2$		4.460	$(6 - (3/2)[\sqrt{3}\sin\beta(\cos\phi - 1) + \cos\beta(\cos\phi + 3)])^{1/2}$
r'_X	O-O	Intertriangle	$2 - 3f/2$		3.217	$(6 - (3/2)[\sqrt{3}\sin\beta(\cos\phi + 1) - \cos\beta(\cos\phi - 3)])^{1/2}$

O-O nearest neighbor peaks to be varied during fitting. Both n_{BO} and $\langle u_{BO}^2 \rangle^{1/2}$ were found to increase approximately linearly with $14 \leq Q_{\max} \leq 24.47 \text{ \AA}^{-1}$, indicating that measurement to even higher Q values would be beneficial. For the chosen $Q_{\max} = 24.47 \text{ \AA}^{-1}$, and at room temperature, we found $n_{BO} = 2.9(2)$ and $\langle u_{BO}^2 \rangle^{1/2} = 0.05(1) \text{ \AA}$. These values are in agreement with the expected $n_{BO} = 3$ and typical values of $\langle u_{BO}^2 \rangle^{1/2}$ from neutron diffraction of 0.043 \AA [21] and 0.06 \AA [27]. Figure 5 shows the temperature dependencies of the peak positions and widths. The B-O bond is seen to expand by $5.1(2) \times 10^{-6} \text{ \AA.K}^{-1}$, which corresponds to an expansion coefficient $\alpha_{BO} = r_{BO}^{-1} \partial r_{BO} / \partial T = 3.7(2) \times 10^{-6} \text{ K}^{-1}$ which is independent of T , within our experimental uncertainty. Table 4 compares α_{BO} with the bulk linear thermal expansion coefficients.

The first sharp diffraction peak (FSDP) at *circa* 1.5 \AA^{-1} in $S(Q)$ (figure 6(c)) was fitted with a Lorentzian lineshape. The reflection of the Lorentzian about $Q = 0$ was included in the fitting, in order to obtain the correct behavior to the low Q side and in the $Q \rightarrow 0$ limit. The extracted widths (ΔQ_{FSDP}) and positions (Q_{FSDP}) are plotted in figures 6(a) and (b) in terms of the correlation lengths ($2\pi/\Delta Q_{\text{FSDP}}$) and periodicities ($2\pi/Q_{\text{FSDP}}$) of the associated intermediate range ordering.

5. Discussion

5.1. B-O bond length thermal expansion

The measured $\alpha_{BO} = 3.7(2) \times 10^{-6} \text{ K}^{-1}$ is smaller than the reported bulk linear expansion coefficients [54] (table 4), which

implies that other mechanisms of expansion are also active. A remarkable feature of liquid B₂O₃ is the fact that its expansion coefficient at high temperature ($\gtrsim 1500 \text{ K}$) is *smaller* than that for the glass, and much smaller than for the liquid close to T_g . This is indicative of a significant structural change, such as the dissolution of boroxol rings with increasing T . As such, α_{BO} accounts for fully one third of the total bulk expansion at 1673 K. In contrast, α_{BO} accounts for only 3% of the total expansion a little above T_g at 684 K. It is of interest to ask how boroxol ring dissolution, as inferred from high temperature Raman spectroscopy [7, 8], might affect the B-O bond thermal expansion? Neutron and x-ray crystallographic studies [62–64] of Cs₂O.9B₂O₃ (one of very few crystals known to contain boroxol rings as part of a continuous borate network) indicate that the in-ring B-O bonds are on average *longer* than the out-of-ring bonds. Nonetheless, their average ($1.363(2) \text{ \AA}$ [64]) is very similar to the B-O bond length within the non-ring triangles in crystalline B₂O₃-I ($1.366(2) \text{ \AA}$ [65, 66]) and on this basis alone, one would not expect boroxol ring dissolution to affect average B-O bond length. However, crystallographically determined bond lengths often require correction for correlated thermal motion [67, 68] and so this conclusion is not definitive. On the other hand, an increase in B-O-B angle, β , upon ring-breaking is expected from ¹¹B NMR measurements on B₂O₃ glass [10], and known correlations between β and chemical shift [69]. Since larger M-O-M bond angles typically lead to shorter M-O bond lengths [70], one should expect a *negative* contribution to α_{BO} . Note that this correlation between bond length and bond angle may explain the observation, both experimental [62] and theoretical [41], of longer B-O bonds inside boroxol ring units. Since we observe

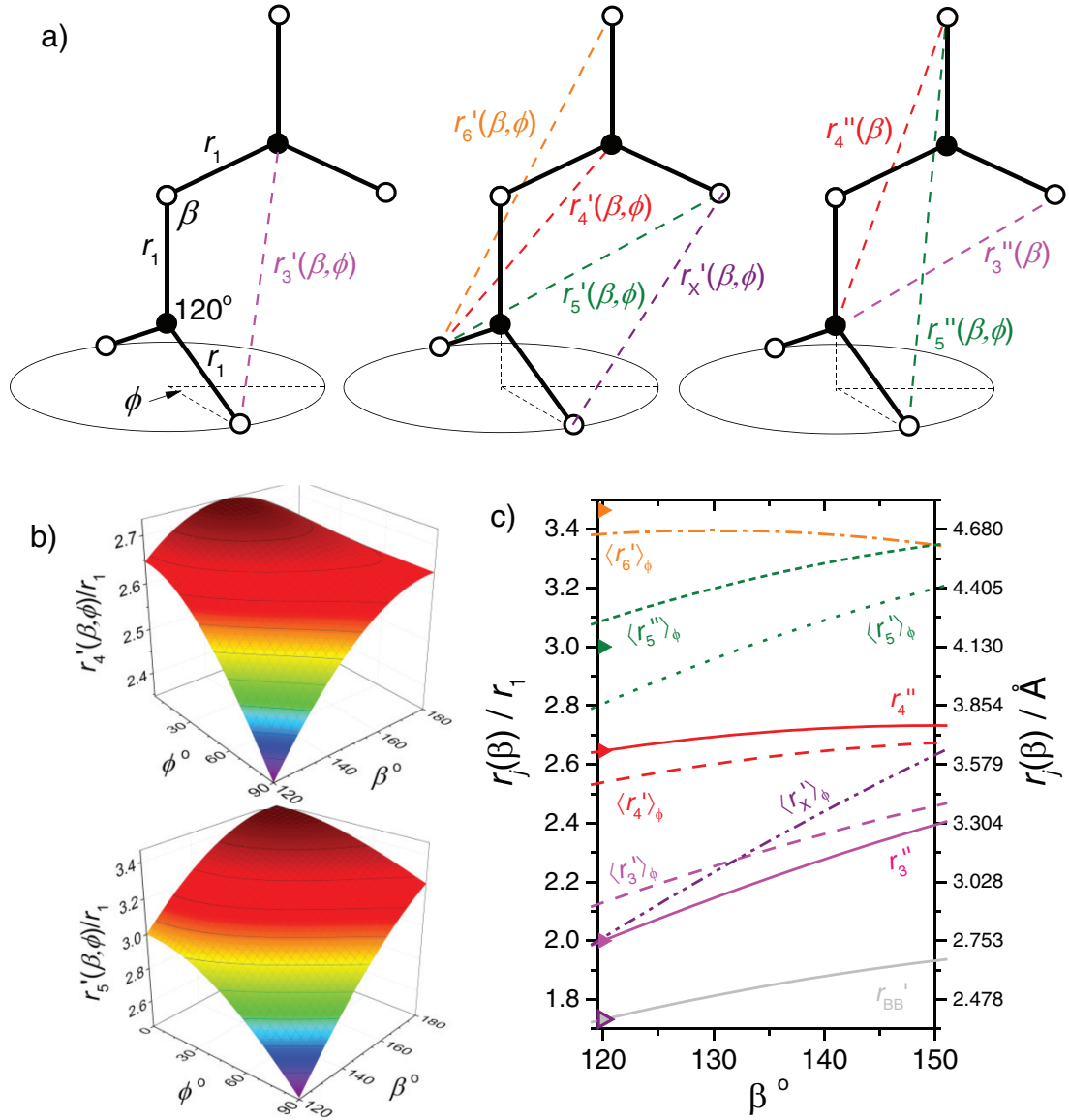


Figure 4. (a) Definitions of the B-O-B bond angle β , and the torsion angle ϕ . General interatomic distances $r_j'(\beta, \phi)$ are also shown, see table 3 for their functional forms and average values. (b) Symmetry inequivalent sections of the $r_j'(\beta, \phi)/r_1$, $j = 4, 5$, surfaces, showing that r_j' can be either larger or smaller than r_j , for $j = 4, 5$, depending upon the combination of β and ϕ . The boroxol distances ($\beta = 120^\circ$, $\phi = 0$) can be seen to the left hand side of each plot. (c) Interatomic distances of part (a) plotted as functions of β . Those denoted $\langle r_j \rangle_\phi$ have been averaged over $\phi \in [0, \pi/2]$. Triangles at $\beta = 120^\circ$ denote the intact boroxol ring distances ($\phi = 0$).

α_{BO} to be positive, we conclude that usual thermal expansion due to anharmonicity of the B-O interaction must dominate, and that other aspects of the diffraction data must be looked to for any evidence of boroxol ring dissolution.

From figure 5(a) it can be seen that the peak position R_2 , which arises primarily from nearest neighbor O-O distances, does not increase linearly. An analogous observation has been made by neutron diffraction [27]. Since, for trigonal planar $[\text{BO}_3]$ triangles, $r_{OO} = \sqrt{3} \cdot r_{BO}$, the observed linear expansion of r_{BO} is expected to give rise to linear expansion of r_{OO} . The discrepancy can be resolved if one attributes the shift to the small contribution from B-B nearest neighbors. However, a shift to larger B-B distances implies larger B-O-B angles, and this is consistent with boroxol ring dissolution, given that

out-of-ring angles, β_{NR} , are greater than in-ring angles, β_R , as implied by ^{11}B NMR [10] and first principles calculations [4] for B_2O_3 glass.

5.2. Intermediate range order

With increasing temperature, the intermediate range ordering (IRO) implied by the FSDP decays approximately linearly (figure 6(a)). Meanwhile the periodicity, $2\pi/Q_{\text{FSDP}}$, (figure 6(b)) increases non-linearly. The latter quantity should be related to the atomic number density, ρ , by $2\pi/Q_{\text{FSDP}} = k_n \rho^n$, where k_n are constants and n is an inverse dimensionality, with $n = 1/3$ for locally isotropic order, $n = 1/2$ for locally chain-like order and $n = 1$ for locally sheet-like order. Misawa [27]

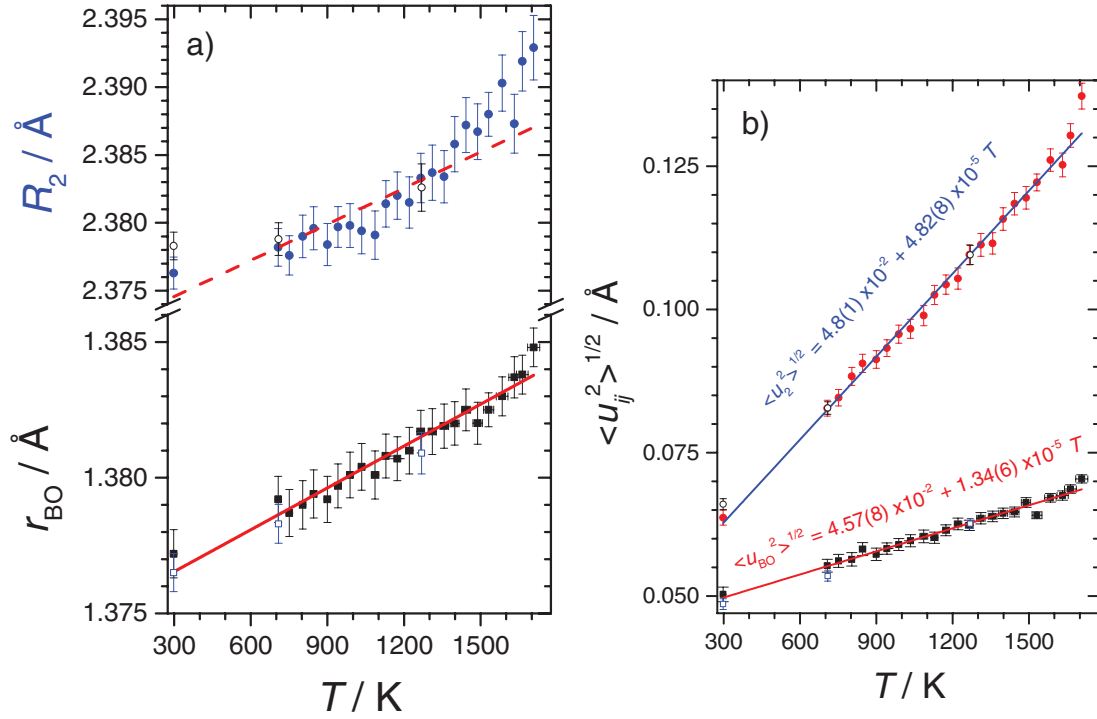


Figure 5. Temperature dependencies of (a) the first two peak positions $R_1 = r_{\text{BO}}$ and $R_2 \approx r_{\text{OO}}$, from peak fitting. The solid line is a linear least-squares fit to the data given by $r_{\text{BO}} = 1.375(3) + 5.1(2) \times 10^{-6} T$ (K), the dashed line is the prediction based on the fit and using $r_{\text{OO}} = 2r_{\text{BO}}\sin(\theta/2)$ with $\theta = 119.2^\circ$. Open symbols denote data taken on cooling, closed symbols on heating. (b) the corresponding peak widths, with linear least-squares fits; error bars in (b) represent statistical errors from fitting only.

has shown using neutron diffraction that, at temperatures close to T_g , a value of $n = 1/3$ is appropriate, but at higher T there is a shift toward higher n . Following Misawa, we have scaled curves for various n , based on literature density measurements [54], to our 707 K value for $2\pi/Q_{\text{FSDP}}$ (figure 6(b)). It is evident that no single value of n is appropriate, with the data laying somewhere between $1/2 < n < 1$. This implies that there is a continuous structural transition, away from isotropic intermediate range order at low T , through chain-like, and toward sheet-like local ordering at very high T . Since IRO in network oxides is typically interpreted in terms of cages of atoms surrounding voids [71], the change in dimensionality inferred from figure 6(b) is to be interpreted in terms of these cages, and not in terms of the underlying network. The break-up of boroxol rings might contribute to such a transition, since this leads to larger rings/chains capable of elongation (e.g. figure 7), but any quantitative link between f and IRO is far from obvious.

5.3. Geometrical model

Following Mozzi and Warren [20] and Hannon *et al* [21], we have constructed a partial geometrical model for the short to intermediate range structure of B_2O_3 . The model is based on the well-established trigonal planar geometry of the $[\text{BO}_3]$ triangle. Here we explicitly consider 1st neighbor B-O, O-O and B-B distances and 2nd neighbor B-O and O-O distances, which depend on, at most, a single B-O-B angle, β , and dihedral angle ϕ (figure 4(a)). Table 3 gives a description of these interatomic distances, which, in general are denoted $r'_j(\beta, \phi)$.

Table 4. Comparison of the measured B-O bond length thermal expansion to the reported bulk linear thermal expansion, $\alpha_L = \alpha_V/3$ [54], at different temperatures.

Temperature (K)	Linear thermal expansion coefficient α_L (10^{-6} K^{-1})	
	B-O bond	Bulk [54]
298 (Glass)	3.7(2)	19.3
684 (Melt)	3.7(2)	111.7
1673 (Melt)	3.7(2)	11.1

For the special case of boroxol rings, the distances are denoted simply by $r_j = r'_j(120^\circ, 0)$. For the r_j , we have followed the numerical indexing system of Hannon *et al* [21]. We note that, whilst for boroxol rings the shortest intraring O-O distance is coincident with the distance r_2 , this does not hold in general, and so we have introduced the distance r'_X which is defined in figure 4(a), and satisfies $r'_X(120^\circ, 0) = r_X = r_2$. Further, we note that for any pair of $[\text{BO}_3]$ triangles sharing a common O atom, there exist pairs of correlated distances, $r_3''(\beta) = r_3'(\beta, 0)$, $r_4''(\beta) = r_4'(\beta, 0)$ and $r_5''(\beta, \phi) = r_5'(-\beta, \phi)$, see figure 4(a). Within this numbering system for the various interatomic distances, it is necessary only to consider $\beta \leq 180^\circ$, since e.g. $r_3'(\beta, \phi) = r_4'(-\beta, \phi)$, and $\phi \leq 90^\circ$, since by symmetry e.g. $r'_X(\beta, \phi) = r'_X(\beta, -\phi)$ and $r'_6(\beta, \phi) = r'_X(\beta, \phi + \pi)$.

The functional forms of the distances $r'_j(\beta, \phi)$ are given in table 3, and some examples plotted in figure 4(b). Average values $\langle r_j \rangle_\phi = (2/\pi) \int_0^{\pi/2} r'_j(\beta, \phi) d\phi$ are plotted in figure 4(c) as functions of β . However, to build up our model

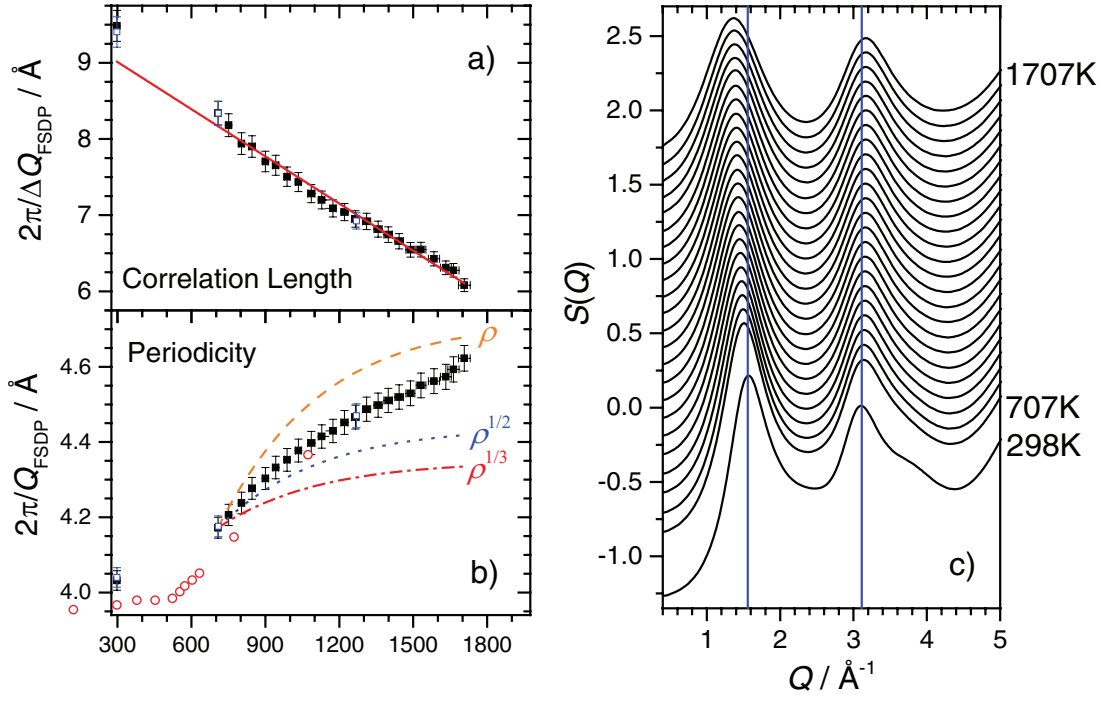


Figure 6. Temperature dependencies of (a) the correlation length and (b) the periodicity derived from Lorentzian fits to the FSDPs, which can be seen at *circa* 1.5 \AA^{-1} in the low Q part of $S(Q)$ shown in (c). The solid line in (a) is a linear least-squares fit to the data. Open symbols denote data taken on cooling, closed symbols on heating. In part (b), the open circles represent the values derived from the neutron diffraction study of Misawa [27]. The various curves in (b) are proportional to ρ^n , and scaled to the data at 707 K. Vertical offsets have been applied in (c) for clarity, and vertical lines are guides to the eye.

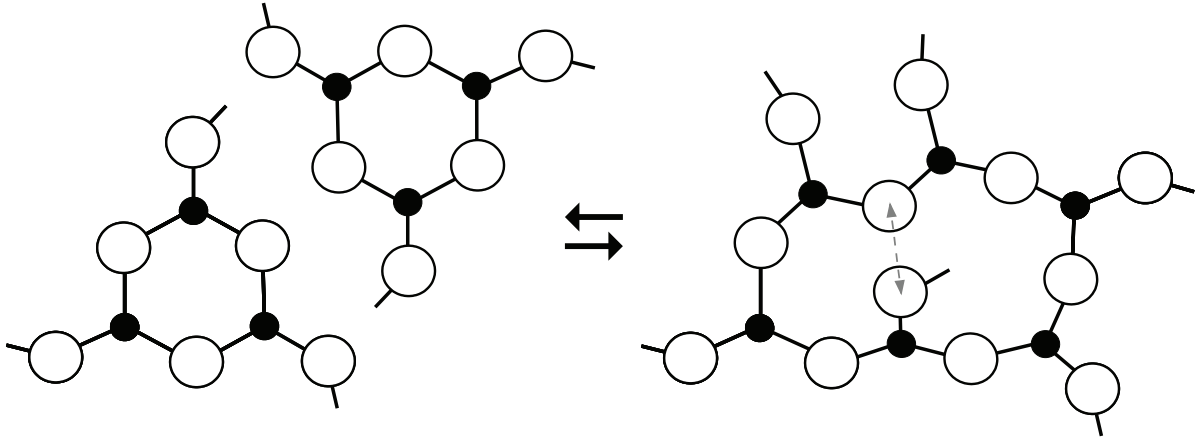


Figure 7. Schematic representation of a possible boroxol ring-breaking mechanism involving the formation of a six-membered ring. The grey dashed arrow within the six-membered ring indicates a 3rd nearest neighbor O-O distance. Note that e.g. the number of 2nd neighbor B-O and O-O distances changes across the transition.

we perform the unweighted averages over $\phi \in [0, \pi/2]$ on the pair functions given by equations (5) to (7), which corresponds to the assumption of a random dihedral angle distribution. The coordination numbers, n_{ij} , are in general functions of the boroxol fraction f , and are given in table 3. We note that the number of atoms considered by the model is not constant, but increases as f decreases due to transitions between e.g. 2nd and 3rd nearest neighbor atoms during boroxol ring rupture (see figure 7).

We next make some simplifying assumptions, in order to obtain a model which depends primarily on the values of f and β_{NR} , for qualitative comparison to the experimental data:

- β within boroxol rings is exactly $\beta_R = 120^\circ$
- β external to boroxol rings, $\beta_{NR} > \beta_R$ as is implied by ^{11}B NMR [10, 69] and first principles calculations [4] for B_2O_3 glass ($\beta_{NR} \approx 135^\circ$)
- The widths of the distributions for the angles β_{NR} & β_R are not explicitly considered, & any disorder is introduced via $\langle u_{ij}^2 \rangle$
- The $\langle u_{ij}^2 \rangle$ are taken from the fitted temperature dependencies shown in figure 5(b), directly for nearest neighbors (with $\langle u_{BB}^2 \rangle = \langle u_{OO}^2 \rangle = \langle u_2^2 \rangle$), whilst for 2nd neighbors, $\langle u_{ij}^2 \rangle = \langle u_2^2 \rangle$ within boroxols, and $\langle u_{ij}^2 \rangle = 2\langle u_2^2 \rangle$ external to

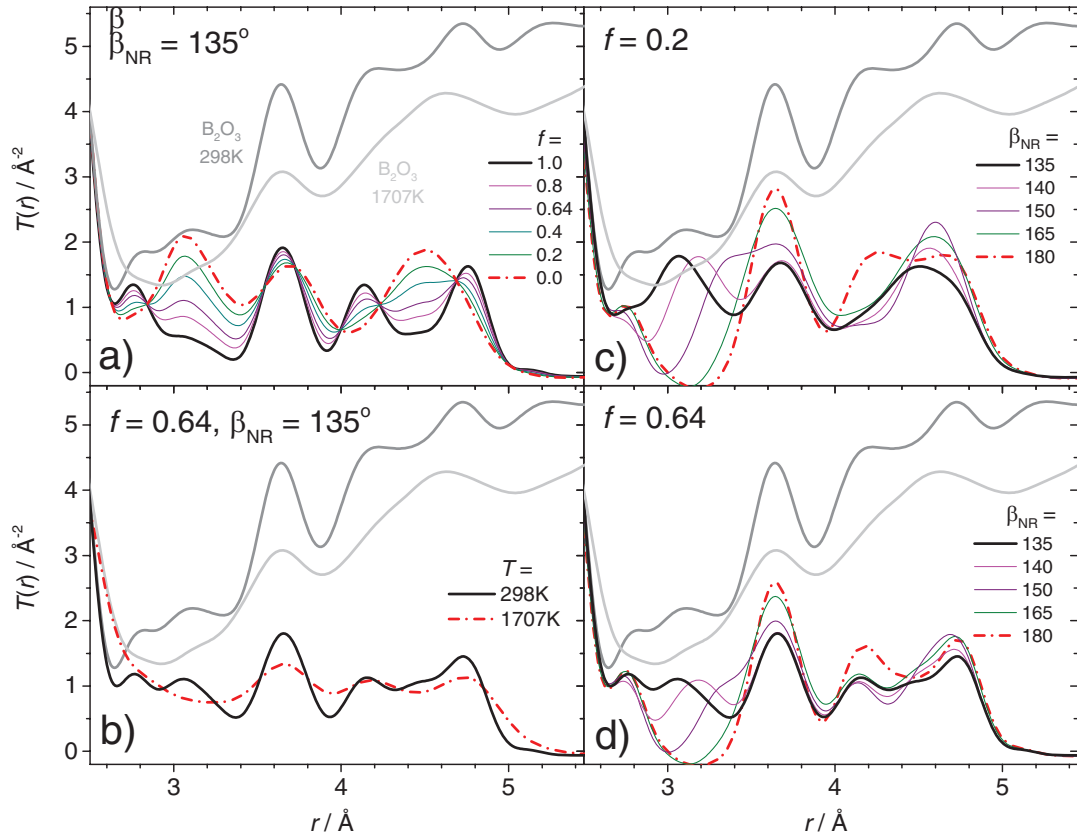


Figure 8. Real-space comparisons of geometrical modelling results and the extremes of the experimental data at $T = 298$ K and 1707 K. In a), c) and d) the model $T = 298$ K is used. $\beta_{\text{NR}} = 135^\circ$ was chosen based on experimental and theoretical determinations for the glass [4, 10], whilst $f = 0.64$ and 0.2 are approximately the low T (glass) and high T limiting values determined by Raman spectroscopy [7].

boroxols, where the factor 2 reflects the empirical relationship between the widths of the distributions of β_{NR} & β_{R} [10]

The model thus has a simple temperature dependence introduced via $r_1(T)$ (figure 5(a)) and the $\langle u_{ij}^2 \rangle(T)$ (figure 5(b)), but otherwise depends only on the variables f and β_{NR} . Of course, one might more correctly integrate over suitable distributions of β , as has been explored using similar models for silica glass [72, 73], but the unknown T dependence of such distributions then introduces additional variables. As such, we rely at first on our simplified model to provide qualitative insight into the dependence of the scattering data on f and β_{NR} , *via* the use of equations (5)–(7), and later discuss its shortcomings and refer to the more complete, space-filling, MD models.

Figure 8 shows some model results obtained for various f , β_{NR} and T , and these are discussed in the following section.

5.4. Boroxol ring dissolution

Since the seminal 1936 study by Warren, Krutter and Morningstar [74], x-ray diffraction, and later neutron diffraction, have both been used many times to study the structure of vitreous (e.g. [3, 20–22, 28]), and occasionally liquid [23–25, 27, 75], B_2O_3 . Most authors infer some sensitivity to boroxol rings, and the majority also infer a large fraction, f , of boron

atoms within such rings, at room temperature. It was not until relatively recently that low values of f were asserted [2, 3] based on empirical structural modelling of diffraction data, and later the sensitivity of diffraction to f has been strongly questioned [42].

Figure 9 shows that the positions of the various peaks in $D(r)$ change with T . Figure 8(a), as well as the arrows in figure 9, show how the peak positions are expected to change if boroxol rings are progressively broken up (as implied by Raman spectroscopy for increasing T [7, 8]), without changes in β_{NR} . Note that the boroxol O-O distance r_6 is the maximum possible value of $r'_6(\beta, \phi)$, such that $r'_6(\beta, \phi) \leq r_6$, and if boroxol rings are broken (f decreases), the observed position, R_6 , should decrease, as observed. For the other peaks the situation is less simple, but if β on average increases upon rupture of a boroxol ring, such that $\beta_{\text{R}} < \beta_{\text{NR}}$ [4, 10], then we can also deduce that $r'_3(\beta, \phi) \geq r_3$. The B-O correlation giving rise to a peak at R_3 is rather weak in x-ray diffraction, and tends to overlap with the large peak at r_2 and also the r'_X O-O peak, and so understanding its influence on $D(r)$ requires more detailed modelling, such as that provided by the MD analysis below. The interatomic distances giving rise to peaks at R_4 and R_5 are more complex, in that they may decrease *or* increase depending on the particular values of $\beta > 120^\circ$ and ϕ , as shown in figure 4(b), and figure 4(c). In the models (figure 8(a)), distances at r_5 tend to be replaced by *larger* distances

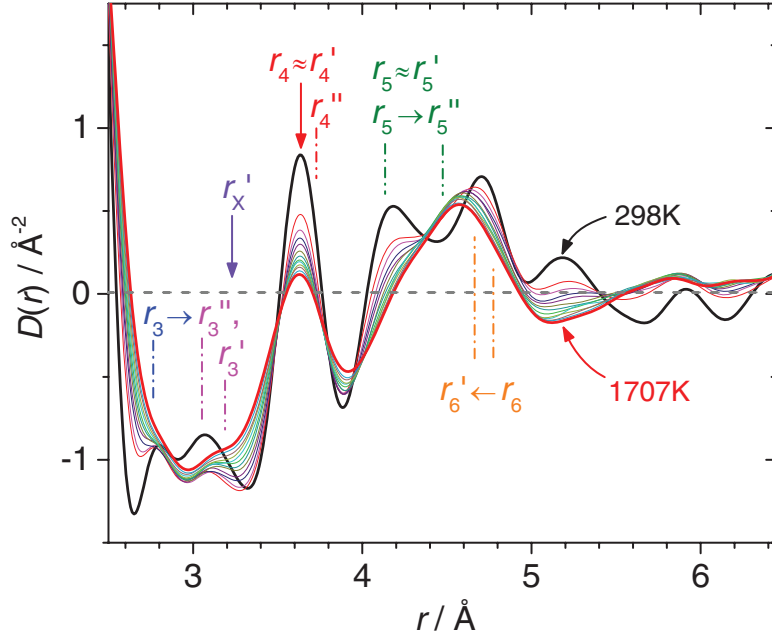


Figure 9. The $D(r)$ for liquid and glassy B_2O_3 from figure 3 ($Q_{\max} = 24.47 \text{ \AA}^{-1}$, with Lorch), shown here overlain, and with every other dataset removed for clarity. Vertical arrows and bars denote average peak positions as calculated based on the geometrical model, and shown in table 3, with $\beta_{NR} = 135^\circ$ (see also figure 4(c)). The horizontal arrows indicate the shifts in peak positions expected for boroxol ring dissolution, which tend to predict the observed changes with increasing temperature.

r_3'' (and similar distances $r_5' \approx r_5$) such that the twin O-O features at $R_5 \approx 4.2 \text{ \AA}$ and $R_6 \approx 4.7 \text{ \AA}$ observed in the glass $D(r)$ merge as f decreases, consistent with the observed trend in the liquid $D(r)$ as T is increased (figure 9). Figure 8(b) shows that such a merging of these peaks does not occur simply due to thermal broadening, where experimental values of f [7] and β_{NR} [10] at room temperature have been used. Figure 8(c) shows that the two peak structure is not obtained at all for low $f = 0.2$ at various β_{NR} (except for the highly unlikely 180° case). Furthermore, figure 8(d) demonstrates that a single peak structure, as observed at high temperatures, cannot be obtained for large $f = 0.64$ simply by changes in the average non-ring B-O-B angle, β_{NR} . From this analysis of expected peak positions, we interpret the observed trends highlighted in figure 9 as clear evidence for boroxol ring dissolution with temperature, and for the qualitative sensitivity of diffraction to the presence of boroxol rings.

One can even look beyond 2nd neighbor correlations, for example, the peak at 5.25 \AA in $D(r)$ (figure 9) can be assigned to a B-O correlation from B in a triangle (or ring) to an O on the far side of an adjacent ring (3rd O neighbor) [20]. This peak diminishes rapidly with T , and is not observed at all at high T , consistent with ring dissolution.

Our conclusion regarding the sensitivity of diffraction to 3-membered rings is in disagreement with a previous study by Soper [42]. We attribute our ability to discern this sensitivity to the collection of high real-space resolution, low noise data from both glass and liquid over a wide temperature range, which allows for the possible variation of f not only in models, but also in the liquid and hence the *experimental diffraction data*. Indeed, such sensitivity was recently claimed using neutron diffraction at high-pressure [43]. Similar to increasing T ,

an increase in P on the room-temperature B_2O_3 glass also leads to the breakdown of boroxol rings and the author's [43] showed that changes in the $2.6 \leq r \leq 3.2 \text{ \AA}$ region of $T(r)$ (r_3 and r_3' B-O peaks) were qualitatively as expected for a reduction in f with increasing P . Finally, we note that the reciprocal space structure factors, $S(Q)$, contain the information sensitive to boroxol rings spread over a wide Q range. Therefore, whilst two $S(Q)$ based on models with very different ring fractions may appear similar, this does *not* imply that there is no information regarding the presence of rings in the data. In fact, if the $S(Q)$ are Fourier transformed to obtain real-space functions, such as $T(r)$, then differences with f become more readily apparent, particularly in the range $2.65 \leq r \leq 5.00 \text{ \AA}$ where several of the intraring peaks appear. We note that Soper's boroxol-rich and boroxol-poor models differ significantly in this region [42].

Fitting of the geometrical models to the $S(Q)$ revealed two qualitative trends, that f decreases with T , as expected from Raman scattering evidence ([7, 8], figure 1) whilst β_{NR} increases with T (see following discussion of MD models).

5.5. Molecular dynamics models

Details of various models closely matching the experimental temperatures and densities (figure 1) are given in table 2. Figure 10 shows some examples of these MD models compared to the real-space diffraction data. Similar trends regarding changes in peak positions with f are observed as with the geometrical model discussed above. In particular the O-O peaks at R_5 and R_6 are separated for large f ($R_5 \approx 4.2 \text{ \AA}$, $R_6 \approx 4.7 \text{ \AA}$), and unresolved for small f (figure 10, 300 K models).

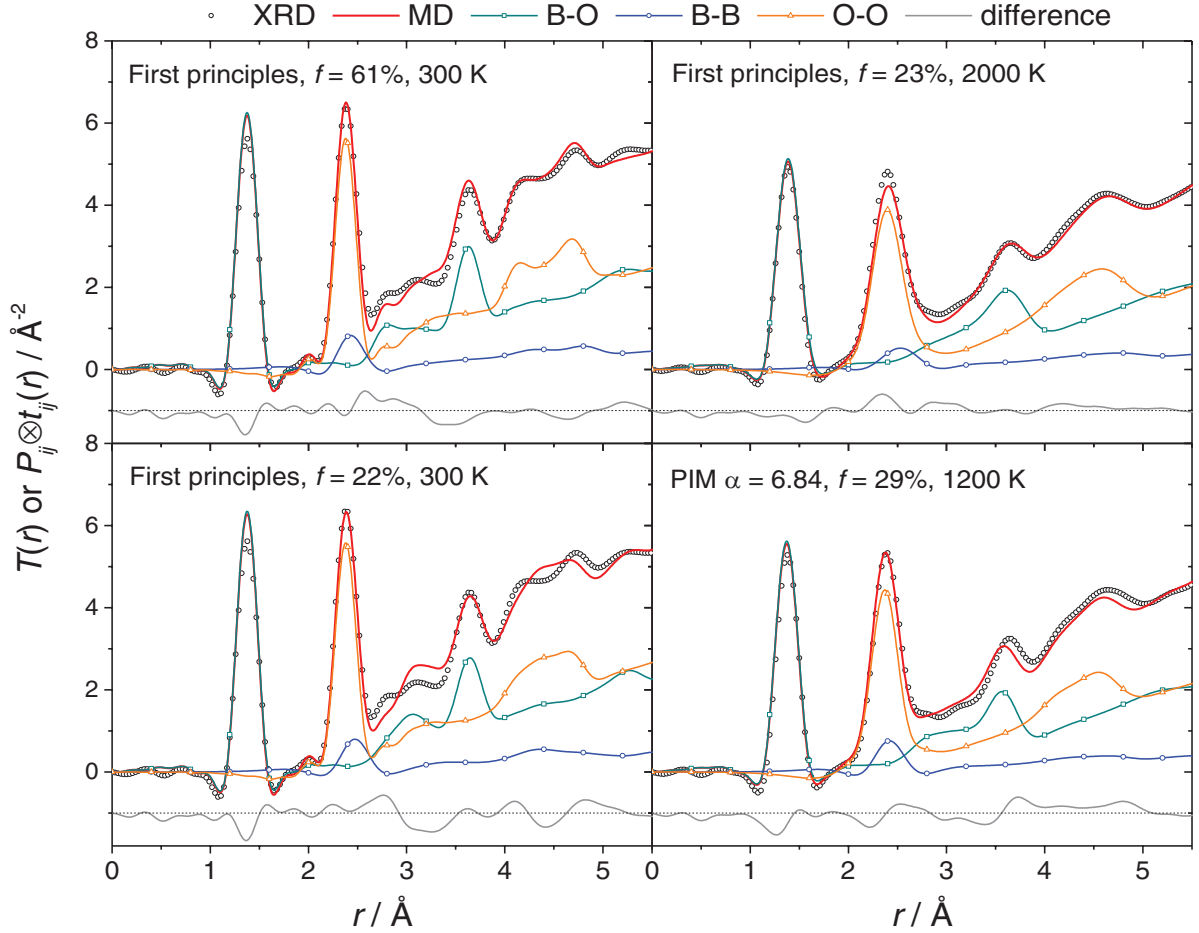


Figure 10. Exemplary total x-ray correlation functions calculated from MD models compared to those experimentally determined by x-ray diffraction. Also shown are the partial pair correlation functions derived from the MD models, and the differences between the model and experimental $T(r)$ are offset below. All functions are convoluted with the x-ray pair functions (equation (7)) using $Q_{\max} = 24.47 \text{ \AA}^{-1}$ with Lorch modification function. Temperatures and f values refer to MD models, see table 2 for full details. The MD functions were calculated using the same densities as for the experimental functions, for better comparison. Additional graphical comparisons available online as supplementary data (stacks.iop.org/JPhysCM/27/455104/mmedia).

In order to judge the comparative agreement of the models with the x-ray diffraction data, the quality-of-fit parameters [76, 77]

$$R_{\chi}(r_1, r_{k,\max}) = \left(\frac{\sum_{k=1}^{k,\max} [T_{\text{exp}}(r_k) - T_{\text{mod}}(r_k)]^2}{\sum_{k=1}^{k,\max} T_{\text{exp}}^2(r_k)} \right)^{1/2}, \quad (9)$$

were calculated, where subscripts exp and mod denote experimental and modelled functions respectively. The range $2.65 \leq r_k \leq 5.00 \text{ \AA}$ was chosen specifically for its sensitivity to the presence of boroxol rings, since it contains the peaks at R_3 through R_6 . The R_{χ} are recorded in table 2 and plotted in figure 11 against the difference between boroxol ring fractions in the models, f_{MD} , and expected from Raman scattering, as given by rearrangement of Walrafen *et al*'s equation (2) [7] to yield

$$f_{\text{Raman}}(T) = A \exp\left(\frac{B}{T} - C\right) \left\{ 1 + \exp\left(\frac{B}{T} - C\right) \right\}^{-1} \quad (10)$$

with $A = 0.644$, $B = 3237.7 \text{ K}$ and $C = 2.589$ (see figure 1). The values $\Delta f = f_{\text{Raman}} - f_{\text{MD}}$ are also given in table 2.

Figure 11 serves to illustrate a number of points. Firstly, there is a positive correlation between R_{χ} and $|\Delta f|$ (adjusted $R^2 = 0.51$, $n = 17$ or $R^2 = 0.74$, $n = 13$ for PIM models only) which itself implies that the diffraction data are indeed sensitive to the boroxol ring fraction. Secondly, an increase in the oxygen polarizability tends to increase the stability of boroxol rings, as noted previously [31, 41], allowing in many cases a closer match between f_{Raman} and f_{MD} . Thirdly, the first-principles results tend to out-perform the PIM model. With regard to this latter point, the B-O-B bond angle distributions shed some light. Table 2 shows the mean B-O-B angles within boroxols $\langle \beta_{\text{R}} \rangle$, and external to boroxols $\langle \beta_{\text{NR}} \rangle$. A key difference is that the first-principles models have larger $\langle \beta_{\text{NR}} \rangle$ compared to the PIM, and this is thought to underlie the larger R_{χ} of the latter (although a marginally shorter B-O bond in the PIM models also contributes). It is also evident that (i) $\langle \beta_{\text{R}} \rangle$ are $< 120^\circ$, implying that there are small distortions from planarity of the boroxol rings, and that these increase in magnitude with T ; (ii) $\langle \beta_{\text{NR}} \rangle$ increases with T as concluded qualitatively by fitting of the geometrical model to the experimental $S(Q)$; (iii) B-O-B angles tend to decrease with increasing oxygen polarizability α .

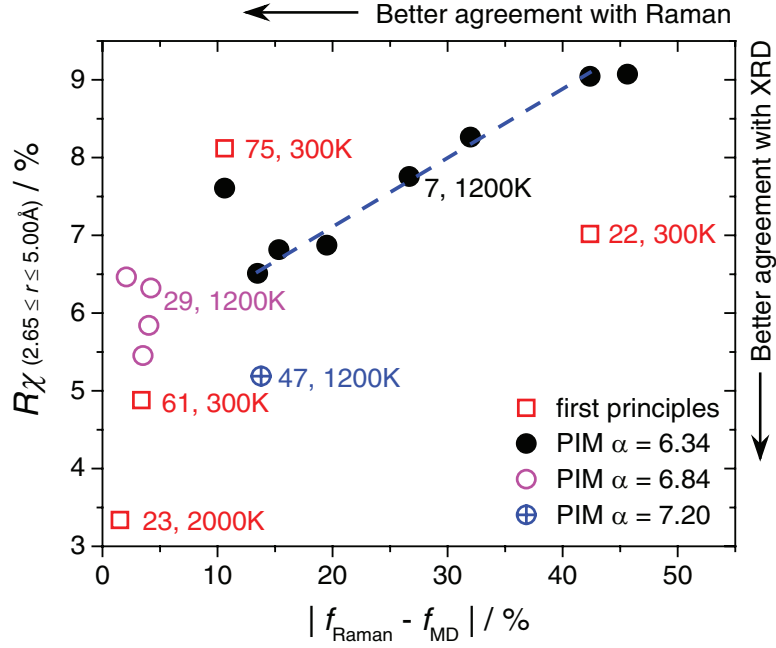


Figure 11. Simultaneous evaluation of MD models against x-ray diffraction and Raman spectroscopy *via* two figures of merit: i) $|\Delta f| = |f_{\text{Raman}} - f_{\text{MD}}|$ (table 2) where f_{Raman} is calculated from Walrafen *et al*'s equation (2) [7], our equation (9), and ii) R_{χ} , equation (10), calculated over the range sensitive to boroxol rings, $2.65 \leq r \leq 5.00 \text{ \AA}$ (table 2). A few points are labelled by their f_{MD} and T_{MD} . The dashed line is a guide to the eye.

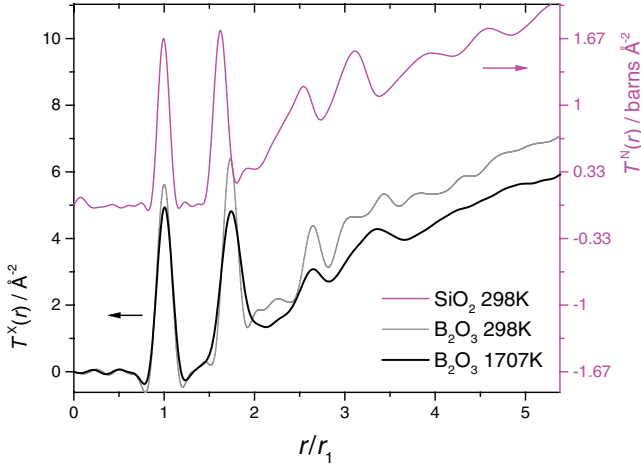


Figure 12. Comparison of $T(r)$ for B_2O_3 melt and glass from x-ray diffraction, with SiO_2 glass from neutron diffraction [87], where the pair weightings happen to be similar. The functions have been scaled to their respective M-O bond lengths, and the same $Q_{\text{max}} = 24.47 \text{ \AA}^{-1}$ was used in all cases. The high- T B_2O_3 melt bears more resemblance to SiO_2 glass than does the B_2O_3 glass, on account of the lower boroxol ring fraction in the melt, and hence its closer similarity to a random network structure, like that of silica.

5.6. Final remarks

At high temperatures, the B_2O_3 liquid, unlike the glass, is close to a random network, with only $f \approx 21\%$ of boron atoms within small 3-membered boroxol rings at $T \approx 1700 \text{ K}$. This is qualitatively more similar to the random network structure originally conceived by Zachariassen [78] for the glass. It is interesting then to compare the high temperature B_2O_3 melt to the prototypical random network glass—silica, SiO_2 . It turns

out that the neutron diffraction weightings for the M-O, O-O and M-M terms for SiO_2 are very similar to the x-ray diffraction weightings for B_2O_3 , and therefore their total correlation functions are compared directly, after scaling to the M-O bond length, in figure 12. Despite the fact that B_2O_3 is based on trigonal planar units, and SiO_2 on tetrahedral units, the high- T B_2O_3 melt bears more resemblance to SiO_2 glass than does the B_2O_3 glass. This in itself provides qualitative evidence for a random network structure of high- T liquid B_2O_3 , as compared to glassy B_2O_3 with its high degree of intermediate range order.

We note that existing evidence from ^{11}B NMR [79] is apparently not in accord with temperature induced boroxol ring dissolution. Maekawa *et al* [79] report an increase in ^{11}B isotropic chemical shift as the temperature of the B_2O_3 melt is increased. This is the opposite to what one would expect based on $\beta_{\text{NR}} > \beta_{\text{R}}$ and known correlations between B-O-B angle and chemical shift [4, 69]. Although there are numerous difficulties with performing NMR at such high temperatures, this effect requires an explanation.

6. Conclusions

We have shown that high-quality x-ray diffraction data, collected from glassy and liquid B_2O_3 over a wide temperature range, are sensitive to the presence of boroxol rings, and are consistent with a gradual dissolution of these rings with increasing temperature. There is analogy with the high pressure dissolution of boroxol rings in B_2O_3 glass, recently also shown to be qualitatively consistent with diffraction data [43]. We have therefore provided independent evidence for boroxol ring dissolution to support the Raman spectroscopic evidence,

which has long stood as the primary experimental support for such a transition. Our conclusion was reached using a combination of (i) an analytical geometrical model with explicit dependence on boroxol ring fraction and non-ring B-O-B angle; (ii) first-principles and polarizable ion model molecular dynamics.

This work therefore supports a role played by boroxol rings in the anomalous temperature dependence of a wide array of physical properties of liquid B₂O₃, such as the density and thermal expansion [54, 57, 80], viscosity [54, 56–58] and the compressibility and elastic moduli [81–84].

Furthermore, we have made a direct measurement of the mean B-O bond thermal expansion in the liquid at $\alpha_{\text{BO}} = 3.7(2) \times 10^{-6} \text{ K}^{-1}$, which is small with respect to the bulk expansion just above the glass transition temperature, but accounts for greater than one third of the bulk expansion at temperatures in excess of 1673 K.

Acknowledgments

Use of the Advanced Photon Source, an Office of Science User Facility operated for the U.S. Department of Energy (DOE) Office of Science by Argonne National Laboratory, was supported by the U.S. DOE under Contract No. DE-AC02-06CH11357. OLGA, JKRW, AT and CJB were supported by U.S. DOE grant No. DE-SC0007564. We wish to thank S Kohara and A C Hannon for access to their numerical datasets from x-ray [3] and neutron [21] diffraction experiments respectively. Support from the French supercomputers (GENCI-CINES/IDRIS: grant x2015081875) and the HPC resources of The Institute for scientific Computing and Simulation (reference ANR-10-EQPX-29-01) are greatly acknowledged. The PhD of AB is supported by French state funds managed by the ANR (under reference ANR-11-IDEX-0004-02) within the framework of the Cluster of Excellence MATISSE.

References

- [1] Ferlat G, Seitsonen A P, Lazzeri M and Mauri F 2012 *Nat. Mater.* **11** 925
- [2] Swenson J and Börjesson L 1997 *Phys. Rev. B* **55** 11138
- [3] Suzuya K, Yoneda Y, Kohara S and Umesaki N 2000 *Phys. Chem. Glasses* **41** 282
- [4] Umari P and Pasquarello A 2005 *Phys. Rev. Lett.* **95** 137401
- [5] Umari P and Pasquarello A 2006 *Phys. Rev. Lett.* **96** 199702
- [6] Swenson J and Börjesson L 2006 *Phys. Rev. Lett.* **96** 199701
- [7] Walrafen G E, Samanta S and Krishnan P 1980 *J. Chem. Phys.* **72** 113
- [8] Hassan A K, Torell L M, Borjesson L and Doweidar H 1992 *Phys. Rev. B* **45** 12797
- [9] Sinclair R N *et al* 2000 *Phys. Chem. Glasses* **41** 286
- [10] Hung I, Howes A P, Parkinson B G, Anupold T, Samoson A, Brown S P, Harrison P F, Holland D and Dupree R 2009 *J. Solid State Chem.* **182** 2402
- [11] Joo C, Werner-Zwanziger U and Zwanziger J W 2000 *J. Non-Cryst. Solids* **271** 265
- [12] Joo C, Werner-Zwanziger U and Zwanziger J W 2000 *J. Non-Cryst. Solids* **261** 282
- [13] Youngman R E and Zwanziger J W 1994 *J. Non-Cryst. Solids* **168** 293
- [14] Jellison G E, Panek L W, Bray P J and Rouse G B 1977 *J. Chem. Phys.* **66** 802
- [15] Wong A, Howes A P, Parkinson B, Anupold T, Samoson A, Holland D and Dupree R 2009 *Phys. Chem. Chem. Phys.* **11** 7061
- [16] Ferlat G, Charpentier T, Seitsonen A P, Takada A, Lazzeri M, Cormier L, Calas G and Mauri F 2008 *Phys. Rev. Lett.* **101** 065504
- [17] Barrio R A, Kerner R, Micoulaut M and Naumis G G 1997 *J. Phys.: Condens. Matter* **9** 9219
- [18] Micoulaut M, Kerner R and Santos-Loff D M *et al* 1995 *J. Phys.: Condens. Matter* **7** 8035
- [19] Santos-Loff D M D, Micoulaut M and Kerner R 1994 *Europhys. Lett.* **28** 573
- [20] Mozzi R L and Warren B E 1970 *J. Appl. Cryst.* **3** 251
- [21] Hannon A C, Grimley D I, Hulme R A, Wright A C and Sinclair R N 1994 *J. Non-Cryst. Solids* **177** 299
- [22] Chason E and Spaepen F 1988 *J. Appl. Phys.* **64** 4435
- [23] Sakowski J and Herms G 2001 *J. Non-Cryst. Solids* **293** 304
- [24] Herms G and Sakowski J 2006 *Phys. Chem. Glasses: Eur. J. Glass Sci. Technol. B* **47** 455
- [25] Strong S L 1965–66 *PhD Thesis* MIT
- [26] Krogh-Moe J 1969 *J. Non-Cryst. Solids* **1** 269
- [27] Misawa M 1990 *J. Non-Cryst. Solids* **122** 33
- [28] Johnson P A V, Wright A C and Sinclair R N 1982 *J. Non-Cryst. Solids* **50** 281
- [29] Soppe W, van der Marel C, van Gunsteren W F and den Hartog H W 1988 *J. Non-Cryst. Solids* **103** 201
- [30] Teter M 1997 *Proc. of the Second Int. Conf. on Borate Glasses, Crystals, and Melts* (Abingdon, United Kingdom: DTIC Document)
- [31] Maranas J K, Chen Y, Stillinger D K and Stillinger F H 2001 *J. Chem. Phys.* **115** 6578
- [32] Fernández-Perea R, Bermejo F J and Senent M 1996 *Phys. Rev. B* **54** 6039
- [33] Fernández-Perea R, Bermejo F and Enciso E 1996 *Phys. Rev. B* **53** 6215
- [34] Xu Q, Kawamura K and Yokokawa T 1988 *J. Non-Cryst. Solids* **104** 261
- [35] Verhoef A and Den Hartog H 1994 *J. Non-Cryst. Solids* **180** 102
- [36] Soppe W and den Hartog H W 1989 *J. Non-Cryst. Solids* **108** 260
- [37] Takada A, Catlow C R A and Price G D 1995 *J. Phys.: Condens. Matter* **7** 8693
- [38] Verhoef A and Den Hartog H 1991 *Radiat. Eff. Defects Solids* **119** 493
- [39] Verhoef A and Den Hartog H 1992 *J. Non-Cryst. Solids* **146** 267
- [40] Soppe W and den Hartog H 1988 *J. Phys. C* **21** L689
- [41] Ferlat G 2015 Rings in network glasses: the B₂O₃ case *Molecular Dynamics Simulations of Disordered Materials* ed C Massobrio *et al* vol 215 (Switzerland: Springer International Publishing) p 367
- [42] Soper A K 2011 *J. Phys.: Condens. Matter* **23** 365402
- [43] Zeidler A *et al* 2014 *Phys. Rev. B* **90** 024206
- [44] Keen D A 2001 *J. Appl. Cryst.* **34** 172
- [45] Lorch E 1969 *J. Phys. C* **2** 229
- [46] Barney E R, Hannon A C, Senkov O N, Scott J M, Miracle D B and Moss R M 2011 *Intermetallics* **19** 860
- [47] Hannon A C and Parker J M 2002 *Physics and Chemistry of Glasses Proc. of the XIX Int. Congress on Glass* vol 43C p 6
- [48] Weber J K R, Krishnan S, Anderson C D and Nordine P C 1995 *J. Am. Ceram. Soc.* **78** 583
- [49] Dimitrov V and Komatsu T 2008 *Phys. Chem. Glasses: Eur. J. Glass Sci. Technol. B* **49** 97
- [50] Weber J K R, Felten J J and Nordine P C 1996 *Rev. Sci. Instrum.* **67** 522

- [51] Skinner L B, Benmore C J and Parise J B 2012 *Nucl. Instrum. Methods A* **662** 61
- [52] Hammersley A P, Svensson S O, Hanfland M, Fitch A N and Hausermann D 1996 *High Press. Res.* **14** 235
- [53] Soper A K and Barney E R 2011 *J. Appl. Cryst.* **44** 714
- [54] Napolitano A, Macedo P B and Hawkins E G 1965 *J. Am. Ceram. Soc.* **48** 613
- [55] Lower N P, McRae J L, Feller H A, Betzen A R, Kapoor S, Affatigato M and Feller S A 2001 *J. Non-Cryst. Solids* **293–295** 669
- [56] Macedo P B and Napolitano A 1968 *J. Chem. Phys.* **49** 1887
- [57] Mackenzie J D 1959 *J. Phys. Chem.* **63** 1875
- [58] Riebling E 1966 *J. Am. Ceram. Soc.* **49** 19
- [59] Huang L and Kieffer J 2006 *Phys. Rev. B* **74** 224107
- [60] Rotenberg B, Salanne M, Simon C and Vuilleumier R 2010 *Phys. Rev. Lett.* **104** 138301
- [61] Baroni A, Pacaud F, Ferlat G, Micoulaut M, Delaye J M, Zeidler A, Salmon P S, Alexander O and Salanne M In preparation
- [62] Haworth R, Wright A C, Sinclair R N, Knight K S, Vedishcheva N M, Polyakova I G and Shakhmatkin B A 2006 *Phys. Chem. Glasses: Eur. J. Glass Sci. Technol. B* **47** 352
- [63] Penin N, Touboul M and Nowogrocki G 2003 *J. Solid State Chem.* **175** 348
- [64] Wright A C, Sinclair R N, Stone C E, Knight K S, Polyakova I G, Vedishcheva N M and Shakhmatkin B A 2003 *Phys. Chem. Glasses* **44** 197
- [65] Effenberger H, Lengauer C L and Parthé E 2001 *Monatsh. Chem.* **132** 1515
- [66] Gurr G, Montgomery P, Knutson C and Gorres B 1970 *Acta Crystallogr. B* **26** 906
- [67] Bubnova R S and Filatov S K 2013 *Z. Kristallogr. Cryst. Mater.* **228** 395
- [68] Dove M T, Keen D A, Hannon A C and Swainson I P 1997 *Phys. Chem. Miner.* **24** 311
- [69] Alderman O L G, Iuga D, Howes A P, Pike K J, Holland D and Dupree R 2013 *Phys. Chem. Chem. Phys.* **15** 8208
- [70] Boisen M B, Gibbs G V, Downs R T and Darco P 1990 *Am. Mineral.* **75** 748
- [71] Wright A C 2008 *Phys. Chem. Glasses: Eur. J. Glass Sci. Technol. B* **49** 103
- [72] Mozzi R and Warren B 1969 *J. Appl. Cryst.* **2** 164
- [73] Poulsen H F, Neufeind J, Neumann H B, Schneider J R and Zeidler M D 1995 *J. Non-Cryst. Solids* **188** 63
- [74] Warren B E, Krutter H and Morningstar O 1936 *J. Am. Ceram. Soc.* **19** 202
- [75] Zarzycki J 1978 Diffraction analysis of vitreous and molten B₂O₃ *Borate Glasses* ed L D Pye *et al* vol 12 (US: Springer) p 201
- [76] Wright A C 1993 Neutron and x-ray amorphography *Experimental Techniques of Glass Science* ed C J Simmons and O H El-Bayoumi (Westerville, OH: The American Ceramic Society) p 205
- [77] Alderman O L G, Skinner L B, Benmore C J, Tamalonis A and Weber J K R 2014 *Phys. Rev. B* **90** 094204
- [78] Zachariasen W H 1932 *J. Am. Chem. Soc.* **54** 3841
- [79] Maekawa H, Inagaki Y, Shimokawa S and Yokokawa T 1995 *J. Chem. Phys.* **103** 371
- [80] Macedo P B, Capps W and Litovitz T A 1966 *J. Chem. Phys.* **44** 3357
- [81] Capps W, Macedo P B, O'Meara B and Litovitz T A 1966 *J. Chem. Phys.* **45** 3431
- [82] Macedo P and Litovitz T A 1965 *Phys. Chem. Glasses* **6** 69
- [83] Kieffer J 2009 *Phys. Chem. Glasses: Eur. J. Glass Sci. Technol. B* **50** 294
- [84] Bockris J O M and Kojonen E 1960 *J. Am. Chem. Soc.* **82** 4493
- [85] Waasmaier D and Kirfel A 1995 *Acta Crystallogr. A* **51** 416
- [86] Shartsis L, Capps W and Spinner S 1953 *J. Am. Ceram. Soc.* **36** 35
- [87] Alderman O L G, Hannon A C, Holland D, Feller S, Lehr G, Vitale A J, Hoppe U, Von Zimmermann M and Watenphul A 2013 *Phys. Chem. Chem. Phys.* **15** 8506